Soft Matter

# Liquid Interfaces with pH-switchable Nanoparticle Arrays



| | |
|---|---|
| Journal: | *Soft Matter* |
| Manuscript ID | SM-ART-03-2018-000583.R1 |
| Article Type: | Paper |
| Date Submitted by the Author: | 13-Apr-2018 |
| Complete List of Authors: | Srivastava, Sunita; Indian Institute of Technology Bombay, Department of Physics; Brookhaven National Laboratory, Center for Functional Nanomaterials<br>Fukuto, Masafumi; Brookhaven National Laboratory, Condensed Matter Physics and Materials Science Department and National Synchrotron Light Source II<br>Gang, Oleg; Brookhaven National Laboratory, Center for Functional Nanomaterials; Columbia University, Department of Chemical Engineering; Columbia University, Department of Applied Physics and Applied Mathematics |
| | |

# Liquid Interfaces with pH-switchable Nanoparticle Arrays

*Sunita Srivastava[1,2], Masafumi Fukuto[3] and Oleg Gang[2,4,5*]*

[1]Department of Physics, Indian Institute of Technology Bombay, Mumbai, 400076, India.

[2]Center for Functional Nanomaterials, Brookhaven National Laboratory, Upton, NY, 11973, USA.

[3]Condensed Matter Physics and Materials Science Department and National Synchrotron Light Source II, Brookhaven National Laboratory, Upton, NY, 11973, USA.

[4]Department of Chemical Engineering, Columbia University, New York, NY, 10027, USA

[5]Department of Applied Physics and Applied Mathematics, Columbia University, New York, NY, 10027, USA

Keywords: Self-assembly, Responsive nanostructures, Liquid interfaces, DNA, Nanoparticles

Stimuli-responsive 2D nanoscale systems offer intriguing opportunities for creating switchable interfaces. At liquid interfaces, such systems can provide a control over interfacial energies, surface structure, rheological and transport characteristics, which is relevant, for example, to bio- and chemical reactors, microfluidic devices, and soft robotics. Here, we explore the formation of pH-responsive membrane formed from gold nanoparticles grafted with DNA (DNA-NPs) at a liquid-vapor interface. DNA-NPs 2D hexagonal lattice can be reversibly switched by pH modulation between an expanded state of non-connected nanoparticles at neutral pH and a contracted state of linked nanoparticles at acidic pH due to the $AH^{+}$-$H^{+}A$ base pairing between A-motifs. Our in-situ surface x-ray scattering studies reveal that the reversible lattice contraction can be tuned by the length of pH-activated linkers, with up to ~ *71%* change in a surface area.

Use of DNA as a programmable self-assembly agent provides a powerful approach for the creation of functional nanoscale structures in a highly controlled fashion[1-12]. A well-defined structure of DNA guided nanoparticle assemblies has allowed for revealing the dependence of mechanical[7], rheological[8] and plasmonic[10, 13] properties of nanoscale organizations on their structure. A molecular plasticity of DNA makes these assembly approaches are highly suitable for the construction of stimuli-responsive nanoarchitectures with the regulated transformation of nanoparticle systems[7-12, 14-16]. Stimuli-responsive polymer brushes have been used to facilitate reconfigurable plasmonic, magnetic, thermal, mechanical and transport properties[17-20]. However, in addition to programmable interconnections and structural modularity used for bulk materials, the stimuli-responsive DNA motifs can be used to tailor nanomaterial surfaces[21-23]. The development of means for controlling liquid interfaces is of the particular interest, since they play an important role in processing of nanoscale and biological materials, as well as for application in drug-delivery and cellular targeting. The aim of the present work is to use pH-activated DNA linkers for creation of switchable liquid interfaces using pH triggering.

The Watson-Crick base pairing is one of the most common binding modes for nucleic acids, however, other, non-Watson-Crick pairing, are exist and various motifs, such as G-quadruplex[24, 25], i-motif [22, 26] and poly(rA) with ostensible adenine-adenine base pairs[27] and poly(dA) through protonated adenine bases[28-30] were reported. In particular, A-motif-based molecular constructs of DNA have been exploited to create a pH-responsive system[29-34], where the formation of $AH^+$-$H^+A$ base pairs occurs at low pH. Such base pairing at low pH offers significant increase in the thermal stability over the traditional Watson-Crick hybridization.

In this study, we demonstrate that pH-triggered DNA motifs can be used for the creation of pH-responsive 2D membrane of DNA-functionalized gold nanoparticles (DNA-NPs) at a liquid-

vapor interface, and such membranes exhibit reversible structural transformations upon pH change in the sub-phase. The in-situ surface scattering reveals 2D hexagonal arrangement of DNA-NPs at neutral pH, and the nanoparticle monolayer is reversibly switched from a state of non-connected nanoparticles in a hexagonal lattice to a contracted lattice (~ 71% change in area) of connected particles by changing pH from *7.4* to *3.5*, respectively.

In Figure 1 we illustrate the system design to achieve the pH-responsive DNA-nanoparticle membrane. We utilize the electrostatic attraction between negatively charged DNA-functionalized gold nanoparticles and a positively charged lipid layer at the liquid-vapor interface to create ordered monolayers of DNA-functionalized gold nanoparticles[8, 9]. The 100% positively charged lipid layer of 1,2-dimyristoy l-3-trimethylammonium-propane (DMTAP, Figure 1a) is prepared by using the Langmuir method with water as the sub-phase solution (see Supporting Materials). Addition of gold nanoparticles (NP) of ~ 8.8±0.8 nm core diameter, functionalized with specifically designed DNA sequences (Table ST1), resulted in the adsorption of the negatively charged DNA-nanoparticles to the lipid layer, thus yielding a nanoparticle monolayer (Figure 1b). After equilibration for ~ 3 hrs for the NP adsorption, a solution of pH-responsive DNA linkers consisting of 15 complementary bases at one end and variable motif for different studied systems with *n* (= *18, 28, 36*) *A*-nucleotide bases on the other end were added to the sub-phase. The complementary segment of the linker is designed to form a double stranded bond with the chains on NP surface through DNA hybridization. The *A*-rich overhangs were incorporated to connect neighboring particles in the 2D NP monolayer by forming the parallel duplex at acidic pH through the reverse Hoogsteen mechanism[29-32]. Addition of NaCl for a final concentration of ~ *10 mM* promot hybridization between the complementary bases of the linkers and the DNA chains on the NP surface. We have established previously that high density of

DNA chains adsorbed at the lipid layer enhances the kinetics of base-pair formation and a salt concentration as low as *10 mM* is sufficient for spontaneous Watson-Crick based complementary DNA hybridization in 2D[8]. After the addition of salt, the sub-phase pH was adjusted to *7.4* using phosphate buffer. This result in a monolayer formation of non-connected NPs whose surface was coated with (pH-responsive) linker-attached DNA chains. After equilibration time of ~ 3-4 hrs to allow salt-driven changes in the DNA-NP layer[9], an excess linkers and nanoparticles in the bulk sub-phase were removed through exchange of the sup-phase solution with salted buffer solution. We refer this as nonactive, $S_N$ state of the DNA-nanoparticle assembly and all pH-driven transformations of the NP monolayer were measured for this state (Figure 1c). Next, to investigate the pH-responsive properties of the DNA-NP membrane, the solution pH was adjusted to *3.5* using sodium citrate buffer, and the linkers at this pH were expected to be in the active state, $S_{A,}$ and to form connections between neighboring particles through the formation of parallel duplex bonds (Figure 1d). Subsequently on changing the solution pH back to *7.4*, the assembly should revert to a monolayer of unconnected nanoparticles, established only by repulsive interactions, with the linkers switching back to the non-activated, $S_N$, state. The in-situ grazing-incidence small-angle x-ray scattering (GISAXS) data, demonstrating the pH-responsive behavior of the DNA-NPs membrane for $S_N$ and $S_A$ state of the assembly with one type of pH-activated linkers (*n= 28*), is shown in Figure 2a. The addition of DNA-coated nanoparticles to the water sub-phase results in the formation of the ordered nanoparticle monolayer, as revealed by the presence of multiple rod-like diffraction features in the GISAXS pattern. This, together with featureless GISAXS patterns observed for a control neutral lipid layer (Figure S1), demonstrates that the electrostatic attraction between the positively charged lipid layer and the DNA-coated nanoparticles and the electrostatic repulsion between particles drive the formation

of ordered 2D nanoparticle arrays at the air-liquid interface. The data for initial stage of nanoparticle adsorption and control sample containing T rich DNA is shown in Figure S2. For the $S_N$ state of the assembly, the positions of the diffraction peaks in the structure factor, $S(q_r)$, profiles (obtained as $S(q_r) = I(q_r)/F(q_r)$, where $F(q_r)$ is a particle form factor measured for the free nanoparticles dispersed in solution and $q_r$ is the surface-parallel component of the scattering wave vector), satisfy the condition for 2D hexagonal lattice, with $q_i / q_{10} \sim 1:\sqrt{3}:\sqrt{4}:\sqrt{7}:\sqrt{9}$ ($q_{10}$ is the peak position for the (10) diffraction plane and $i$ is the peak index corresponding to the diffraction peaks from (10), (11), (20), and higher order planes), in agreement with previous observations[5, 6, 8, 9, 13, 35]. Detailed structural analysis of the GISAXS data reveals an in-plane interparticle distance, $d$, of $44.3nm$ calculated as $4\pi/\sqrt{3}q_{10}$, for $S_N$ state of the nanoparticle monolayer ($n$ = 28).

Subsequently, the lowering of the sub-phase pH to ~ *3.5*, which brought the system to the activated linker state, $S_A$, resulted in significant change in the scattering line profile. As shown in Figure 2a, the switch from $S_N$ to $S_A$ caused a shift in the first diffraction peak towards higher $q$, corresponding to $d \sim 24.9\ nm$ for $S_A$, which is a ~ *44%* reduction in the in-plane interparticle distance comparing to the $S_N$ state ($n$ = 28). We find that the systems with linker length $n$= 18 and 28, also exhibited highly ordered 2D hexagonal nanoparticle lattices, albeit with different in-plane interparticle distances and correlation lengths (Figure S3). For the system with linker length, n=36, we measure slight broadening in the diffraction peaks, which may arise from the lattice being softer for longer DNA chains. For the systems with $n$ = 18 and 36, we measured ~*39%* and ~*47%* reduction in the in-plane interparticle distance, respectively (Supporting Materials). Subsequently, on switching the sub-phase pH back to *7.4* to revert the system to the

non-activated linker state, $S_{N,}$ the diffraction line profile exhibits reverse change, corresponding to an increase in the inter-particle spacing to *44.3 nm* (Figure 2b). We performed measurements on a control sample, for which a DNA linker is designed to be rich in poly(T) bases (Supporting Materials) and, thus, such motif does not form a parallel duplexes under acidic conditions. As shown in Figure S2 for the control system, the 2D NP assembly retains the $S_N$ state of the hexagonal structure with no change in the in-plane interparticle distance upon pH change, confirming that the pH-driven $AH^+$-$H^+A$ base pairing for the *A*-rich DNA linker is a driving force for the observed lattice contraction.

A signature feature of the pH-mediated parallel duplexes is their reversibility due to the formation and dissociation of the *A*-motif bond. Our experiments verifies the reversibility of the structure transformation of the DNA-NP membrane, between the $S_A$ and $S_N$ states, as evident from Figure 2b. Indeed, the transition between the $S_A$ state at pH *3.5* and the $S_N$ state at pH *7.4* can be efficiently cycled with negligible loss in nanoparticle ordering over several pH exchanges. An illustration of the 2D nanoparticle morphologies at non-activated $S_N$ and activated $S_A$ states is shown in the inset of Figure 2b. The molecular structure in Figure 2c shows the reverse the bond formation for the parallel-duplex *A*-motif via Hoogsteen mechanism, where $AH^+$-$H^+A$ base pairing occurs at acidic pH.

To investigate the normal to the surface structure of the NP monolayer at different pH, we performed in-situ x-ray reflectivity (XRR)[36] measurements that provides an electron density distribution of the interface (Supporting Materials). The XRR profiles obtained from the system $n = 28$, at different pH conditions are shown on a semi-log plot as $Iq_z^4$ vs $q_z^4$, where $I$ is the reflectivity signal from a nanoparticle monolayer and $q_z$ is a surface-normal scattering wave

vector. The oscillatory features in XRR profile at high *q* corresponds to the thickness of the lipid monolayer, while the oscillations at low *q* reveals information about the DNA-NP layer (Figure 3a). With change in pH from *7.4* ($S_N$) to *3.5* ($S_A$), there is minor shift in oscillation minima corresponding to lipid layer thickness towards lower scattering wave vector, indicative of an small ~ *3*□ increase in the thickness of a lipid layer. However, we did not observe any changes in the DNA-NP layer, as evident from the XRR scattering data at low $q_z$, which exhibits similar scattering profile at the different pH. To extract quantitaive information about the structure of the surface, we model our data using the Parratt formalism[37, 38] for multiple interfaces. Fits to the data were performed by applying a box model, where separate boxes were introduced to define different physical layers at the interface. Our model consists of multiple boxes to account for the lipid tail of hydrocarbon chain, lipid headgroup, DNA shell in the vicinity of lipid layer, nanoparticle core and particle's DNA shell at the water sub-phase, respectively. Detailed description of the model along with fiting parameter is provided in supplementary materials. The roughness at the lipid and DNA-nanoparticle interface, was allowed to vary to account for any inhomogeneity of the monolayer. Through the fit of XRR data to this model we extract electron density profiles for both the pH conditions, as shown in Figure 3b. The estimate of maximum *e*-density for the lipid monolayer was found to be ~ 0.35e/Å$^3$. This value is slightly higher than that of water ~ 0.33e/Å$^3$ and consistent with the lipid head group[39]. We observed a subtle difference between the morphology of the DNA-NP and lipid layer at $S_N$ and $S_A$ states of the assembly. As pointed earlier the high *q* region for $S_A$ reveals higher amplitude of the oscillation, as compared to $S_N$. This corresponds to changes in the lipid/DNA-NP interface, as indicated by the *e*-density profile, which exhibits a higher contrast and a larger thickness for the lipid/DNA-NP layer. Our analysis suggests that the bond formation between *A*-nucleotides of the pH activated linker may

lead to the formation of the DNA-rich layer (Figure 3c). The DNA layer may act a depletion layer and provide a larger thickness and contrast for a lipid layer in the scattering measurements. Analogously to the in-plane structure, the surface-normal structure measured from XRR, also exhibits reversible structural transformations for the DNA-NP monolayer with a pH change.

The observed changes in the interparticle spacing between the two structural states at pH 7.4 and *3.5* are a result of the formation of a parallel-stranded duplex between the *A*-rich linkers at acidic pH. The linker DNA chains exist as right-handed single helices at pH 7.4 and switch to parallel-stranded duplexes at acidic pH, held by reverse Hoogsteen base-pairing ($AH^+$-$H^+A$) between protonated adenosines, as shown in Figure 2c. In the reverse Hoogsteen base-pairing, which adapts a different geometry than the Watson-crick base pairs, one base in the Hoogsteen face is rotated by $180^o$ with respect to the other allowing the formation of parallel duplex through hydrogen bonds between N6-N7 molecules of the Adenine nucleotides. The parallel duplex bond between Adenine amino protons and Adenine hydrogen protons is further established by strong electrostatic interaction between the phosphate oxygen and N1-protonated adenines at acidic pH, as indicated by the dashed line in Figure 2c.

It is important to note that the lattice symmetry of nanoparticles in the pH-responsive NP membrane remains hexagonal during all stages of the nanoparticle assembly, as confirmed by the peak position ratios in the GISAXS data. The observed scenario for the pH-driven connection between DNA-NPs is remarkably different from the situation in which DNA-NPs connect through DNA sequence complementarity. The pH-driven process is based on only one kind of nanoparticles with identical DNA chains, which, when arranged in a 2D hexagonal lattice, can connect to all neighboring particles through the formation of *A*-motifs.

The responsiveness of nanoparticle membrane to the pH change can be tuned by varying the length of the connecting *A* nucleotides bases in the DNA linker. The difference between the in-plane interparticle distance, *d*, for the $S_N$ and $S_A$ states of the DNA-NP membrane increases with the length of the pH-responsive linker (Figure 4a). For the system with *n=18* we measure a ~ *39%* change in the in-plane interparticle distance, which increases to ~ *47%* for the system with *n=36.* Additionally, we find that for all linker length *n*, the measured value of the in-plane distance for the $S_N$ state is consistently lower than the estimate based on the worm-like chain model [40] for polymeric chains in solution (Figure S5). This observation is counterintuitive, since one would expect an increase in the inter-particle distance due to large excluded-volume interactions between DNA chains in the confined geometry for 2D systems as compared to bulk. However, this expectation is satisfied for the state of the assembly, when no linker chains are present: the measured in-plane distance is larger than predicted by the worm-like chain model (Supporting Materials). Another intriguing observation is the significant decrease in the correlation length, $\xi \sim 2\pi/\Delta q$[41] (where $\Delta q$ is the resolution-corrected full width at half maximum of the first diffraction peak),- a measure of the ordering in the NP assembly-, with the change in pH from *7.4* to *3.5*. As shown in Figure 4b, we observed a five-fold decrease in $\xi$ as the system switched from the $S_N$ to the $S_A$. As shown in Figure S6, the estimate of DNA-NP coverage from GISAXS and XRR are in good agreement, revealing the formation of homogeneous layer. However for $S_A$, GISAXS result is an overestimation revealing the presence of empty areas that arise because of the bond formation between pH activated linkers at the acidic conditions. This effect indicates that the inter-chain bonds impact the extent of long-range ordering in the nanoparticle lattice. For $S_N$, the 2D hexagonal lattice is established by repulsive inter-particle interactions between non-connected nanoparticles, whereas in the $S_A$ state, the pH-driven

formation of *A*-motif dominates and primarily controls the nanoparticle morphology. The resulting decrease in the inter-particle distance might generate empty surface areas under the lipid layer. That is likely to cause defects in the monolayer and, consequently, can explain a significant change in the correlation length of the ordered DNA-NP arrays. In addition, the correlation lengths were found to decrease marginally with increase in the number of pH-responsive bases in DNA linkers.

In conclusion, we have demonstrated the formation of pH-responsive DNA-nanoparticle monolayer membranes at a liquid interface by virtue of adenines. The formation of *A*-motif, parallel-stranded duplex held by the reversible Hoogsteen base-pairing ($AH^+$-$H^+A$) between protonated adenosines, at acidic pH is a driving force for the structural transformation of 2D nanoparticle lattice. The transition between the two distinct states $S_A$ and $S_N$ at pH *3.5* and *7.4,* respectively, is accompanied by a significant (~ *47%)* and reversible change in the lattice constant which can be tuned by the length of the *A*-nucleotides in the pH-responsive part of a DNA linker. Our results present a promising method to construct pH-reversible nanoparticle membranes with tunable interparticle distances, which could find use for regulating the interfacial structure, energies, and transport for the potential rheological, nanomaterial and biomedical applications.

ASSOCIATED CONTENT

GISAXS and X-ray reflectivity data, DNA-NP characterization, data for control experiment and table for DNA sequences used in these studies.

AUTHOR INFORMATION

**Corresponding Author**

**og2226@columbia.edu**

**Author Contributions**

The manuscript was written through contributions of all authors. All authors have given approval to the final version of the manuscript.

**Acknowledgment**

Research carried out at the Center for Functional Nanomaterials, Brookhaven National Laboratory, which is supported by the U.S. Department of Energy, Office of Basic Energy Sciences, under Contract No. DE-AC02-98CH10886. M. F. acknowledges support by the U.S. Department of Energy, Office of Basic Energy Sciences, Division of Materials Sciences and Engineering, under Contract No. DE-AC02-98CH10886, and through the National Synchrotron Light Source II under Contract No. DE-SC0012704. Use of the National Synchrotron Light Source was supported by the U.S. Department of Energy, Office of Basic Energy Sciences, under Contract No. DE-AC02-98CH10886. O. G acknowledges support by the U.S. Department of Energy, Office of Basic Energy Sciences, Division of Materials Sciences and Engineering, under Contract No. DE-SC0008772.

## REFERENCES


1. Alivisatos, A. P.; Johnsson, K. P.; Peng, X. G.; Wilson, T. E.; Loweth, C. J.; Bruchez, M. P.; Schultz, P. G. *Nature* **1996,** 382, (6592), 609-611.
2. Nykypanchuk, D.; Maye, M. M.; van der Lelie, D.; Gang, O. *Nature* **2008,** 451, (7178), 549-52.
3. Park, S. Y.; Lytton-Jean, A. K. R.; Lee, B.; Weigand, S.; Schatz, G. C.; Mirkin, C. A. *Nature* **2008,** 451, (7178), 553-556.
4. Cheng, W. L.; Campolongo, M. J.; Cha, J. J.; Tan, S. J.; Umbach, C. C.; Muller, D. A.; Luo, D. *Nature materials* **2009,** 8, (6), 519-525.
5. Zhang, H. H.; Wang, W. J.; Hagen, N.; Kuzmenko, I.; Akinc, M.; Travesset, A.; Mallapragada, S.; Vaknin, D. *Adv Mater Interfaces* **2016,** 3, (16).
6. Campolongo, M. J.; Tan, S. J.; Smilgies, D. M.; Zhao, M.; Chen, Y.; Xhangolli, I.; Cheng, W. L.; Luo, D. *Acs Nano* **2011,** 5, (10), 7978-7985.
7. Srivastava, S.; Nykypanchuk, D.; Maye, M. M.; Tkachenko, A. V.; Gang, O. *Soft Matter* **2013,** 9, (44), 10452-10457.
8. Srivastava, S.; Nykypanchuk, D.; Fukuto, M.; Halverson, J. D.; Tkachenko, A. V.; Yager, K. G.; Gang, O. *J Am Chem Soc* **2014,** 136, (23), 8323-8332.
9. Srivastava, S.; Nykypanchuk, D.; Fukuto, M.; Gang, O. *Acs Nano* **2014,** 8, (10), 9857-9866.
10. Thacker, V. V.; Herrmann, L. O.; Sigle, D. O.; Zhang, T.; Liedl, T.; Baumberg, J. J.; Keyser, U. F. *Nat Commun* **2014,** 5.
11. Maye, M. M.; Kumara, M. T.; Nykypanchuk, D.; Sherman, W. B.; Gang, O. *Nat Nanotechnol* **2010,** 5, (2), 116-120.
12. Zhang, Y. G.; Pal, S.; Srinivasan, B.; Vo, T.; Kumar, S.; Gang, O. *Nature materials* **2015,** 14, (8), 840-847.
13. Tan, S. J.; Campolongo, M. J.; Luo, D.; Cheng, W. L. *Nat Nanotechnol* **2011,** 6, (5), 268-276.
14. Macfarlane, R. J.; Lee, B.; Jones, M. R.; Harris, N.; Schatz, G. C.; Mirkin, C. A. *Science* **2011,** 334, (6053), 204-208.
15. Dai, Z. W.; Leung, H. M.; Lo, P. K. *Small* **2017,** 13, (7).
16. Clever, G. H.; Kaul, C.; Carell, T. *Angew Chem Int Edit* **2007,** 46, (33), 6226-6236.
17. Lee, H. I.; Pietrasik, J.; Sheiko, S. S.; Matyjaszewski, K. *Prog Polym Sci* **2010,** 35, (1-2), 24-44.
18. Dai, S.; Ravi, P.; Tam, K. C. *Soft Matter* **2009,** 5, (13), 2513-2533.
19. Choi, W. S.; Koo, H. Y.; Kim, J. Y.; Huck, W. T. S. *Adv Mater* **2008,** 20, (23), 4504-4508.
20. Yameen, B.; Ali, M.; Neumann, R.; Ensinger, W.; Knoll, W.; Azzaroni, O. *Nano Lett* **2009,** 9, (7), 2788-2793.
21. Hu, Y. W.; Ren, J. T.; Lu, C. H.; Willner, I. *Nano Lett* **2016,** 16, (7), 4590-4594.
22. Liu, D. S.; Bruckbauer, A.; Abell, C.; Balasubramanian, S.; Kang, D. J.; Klenerman, D.; Zhou, D. J. *J Am Chem Soc* **2006,** 128, (6), 2067-2071.
23. Estephan, Z. G.; Qian, Z. X.; Lee, D.; Crocker, J. C.; Park, S. J. *Nano Lett* **2013,** 13, (9), 4449-4455.
24. Smith, F. W.; Feigon, J. *Nature* **1992,** 356, (6365), 164-168.
25. Alberti, P.; Mergny, J. L. *P Natl Acad Sci USA* **2003,** 100, (4), 1569-1573.

26. Phan, A. T.; Mergny, J. L. *Nucleic Acids Res* **2002,** 30, (21), 4618-4625.
27. Zhao, C.; Peng, Y. H.; Song, Y. J.; Ren, J. S.; Qu, X. G. *Small* **2008,** 4, (5), 656-661.
28. Chakraborty, S.; Sharma, S.; Maiti, P. K.; Krishnan, Y. *Nucleic Acids Res* **2009,** 37, (9), 2810-2817.
29. Wang, C. Y.; Tao, Y.; Pu, F.; Ren, J. S.; Qu, X. G. *Soft Matter* **2011,** 7, (22), 10574-10576.
30. Persil, O.; Santai, C. T.; Jain, S. S.; Hud, N. V. *J Am Chem Soc* **2004,** 126, (28), 8644-8645.
31. Modi, S.; Swetha, M. G.; Goswami, D.; Gupta, G. D.; Mayor, S.; Krishnan, Y. *Nat Nanotechnol* **2009,** 4, (5), 325-330.
32. Saha, S.; Chakraborty, K.; Krishnan, Y. *Chem Commun* **2012,** 48, (19), 2513-2515.
33. Maji, B.; Samanta, S. K.; Bhattacharya, S. *Nanoscale* **2014,** 6, (7), 3721-3730.
34. Huang, Z. C.; Liu, B. W.; Liu, J. W. *Langmuir* **2016,** 32, (45), 11986-11992.
35. Zhang, H. H.; Wang, W. J.; Mallapragada, S.; Travesset, A.; Vaknin, D. *Nanoscale* **2017,** 9, (1), 164-171.
36. Daillant, J., Gibaud, Alain, *X-ray and Neutron ReflectivityPrinciples and Applications*. Springer, Berlin, Heidelberg.
37. Parratt, L. G. *Physics Review* **1954,** 95, 359.
38. Nelson, A. *J Appl Crystallogr* **2006,** 39, 273-276.
39. Yang, L.; Wang, S. T.; Fukuto, M.; Checco, A.; Niu, Z. W.; Wang, Q. *Soft Matter* **2009,** 5, (24), 4951-4961.
40. Doi, M. E., S. F, *The theory of Polymer Dynamics*. Oxford Science Publications: 2001.
41. Warren, B. E., *X-Ray Diffraction*. Addison-Wesley Publishing Company, Inc.: 1969.

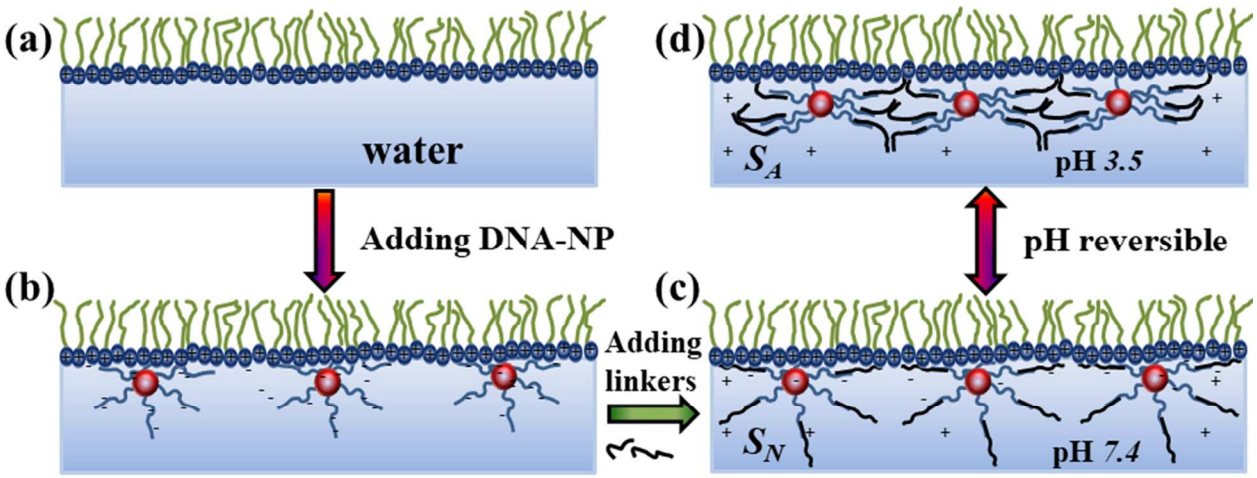


**Figure 1** Schematic step-wise illustration of the experimental procedure for the creation of the pH-responsive 2D DNA-nanoparticle layer at the liquid-air interface (cartoon not to scale). (a) The cationic lipid layer at the air-water interface is created through the Langmuir method. (b) The addition of DNA-functionalized NPs in the sub-phase results in the formation of a nanoparticle monolayer at the interface established through electrostatic interactions between lipids and DNA-NPs. For the linker-attached state, specifically designed pH-responsive linkers are added to the sub-phase.The sub-phase pH is adjusted to 7.4, for the $S_N$ state (c). At acidic pH ~ 3.5, the activated state $S_A$ formed as discussed in the text (d).

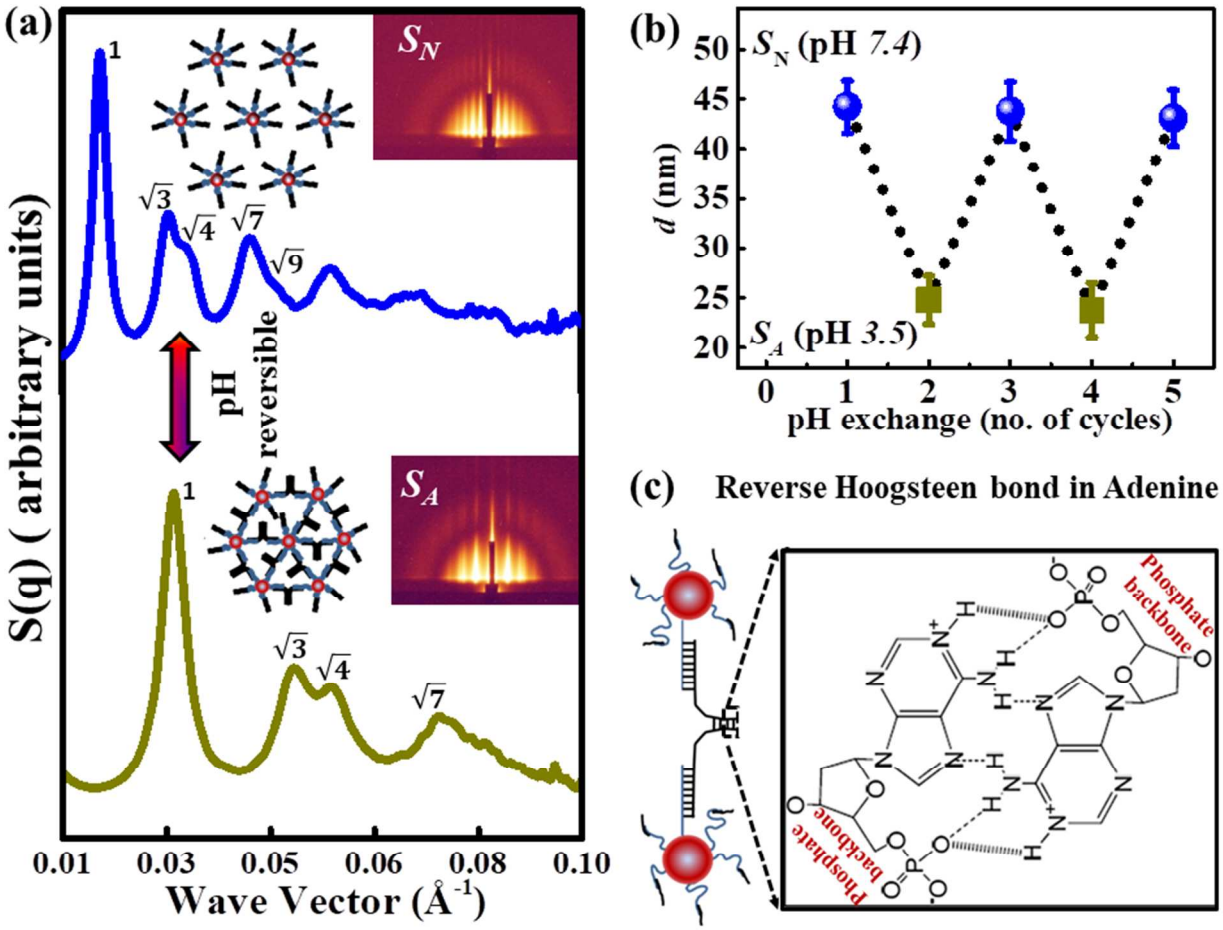


**Figure 2** (a) Structure factor, *S(q),* extracted from 2D GISAXS patterns (inset) for the system with *n =28*, at $S_N$ and $S_A$ , the non-activated state of DNA linkers at pH 7.4 and activated state of linker for pH of 3.5 respectively. Cartoon (inset) illustrating connection between nanoparticles in 2D assembly via DNA linker. (b) The measured in-plane interparticle spacing reversibly switches between non-activated ($S_N$, single) and activated ($S_A$, duplex) DNA chains upon cycling the sub-phase pH between *7.4* (●) and *3.5* (■) respectively. (c) Molecular demonstration of bond formation *via* the reverse Hoogsteen mechanism in *A* nucleotides at acidic pH.

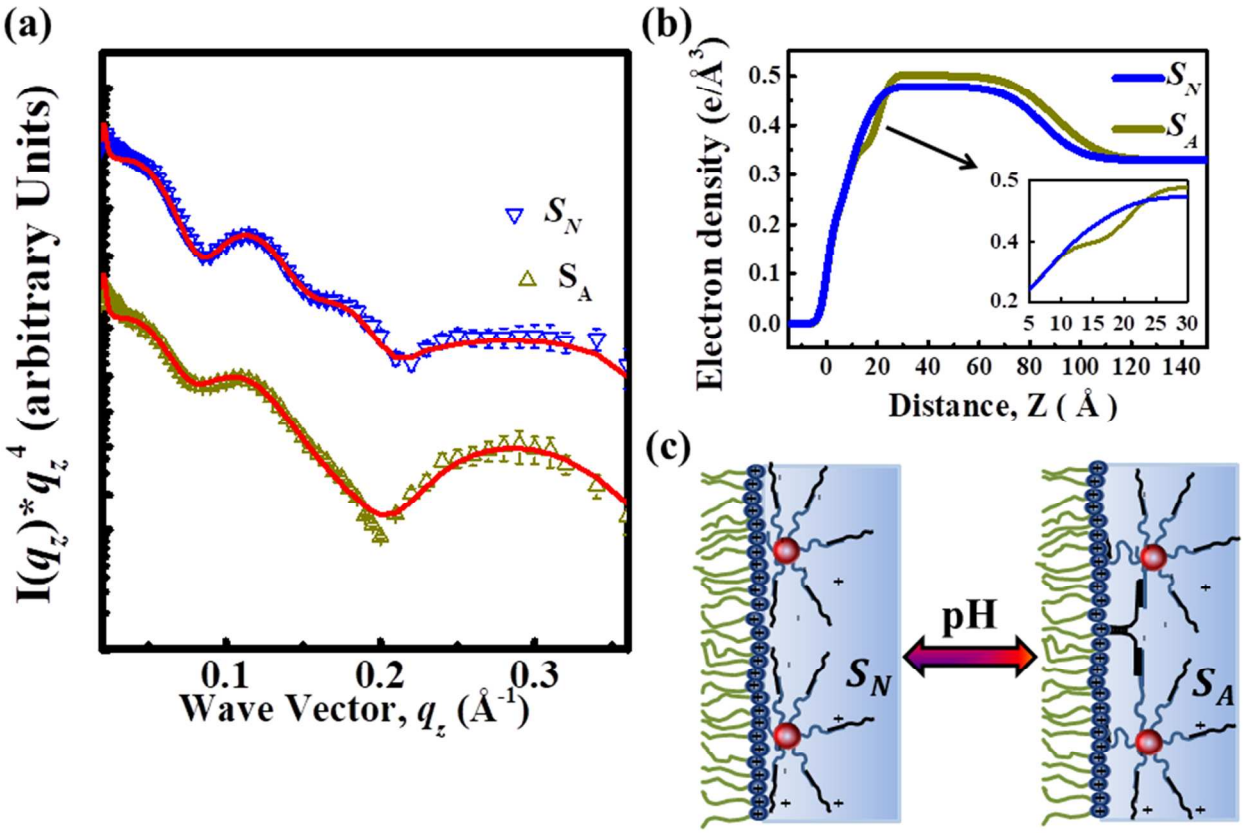


**Figure 3** (a) In-situ x-ray reflectivity (XRR) data for non-activated, $S_N$ (pH 7.4) and activated, $S_A$ states of the pH responsive nanoparticle-membrane. Solid lines are fits to the data using Parratt formalism. (b) The electron density profiles are obtained from fits to data in (a) using a box model, Moto fit-package in Igor Pro[38, 39]. (c) Cartoon showing cross-sectional morphology of the DNA-NP membrane. In pH activated state, DNA linkers connect to form parallel *A*-motif, which act as a depletion layer, suggesting an increase in a thickness and a higher contrast of the lipid layer.

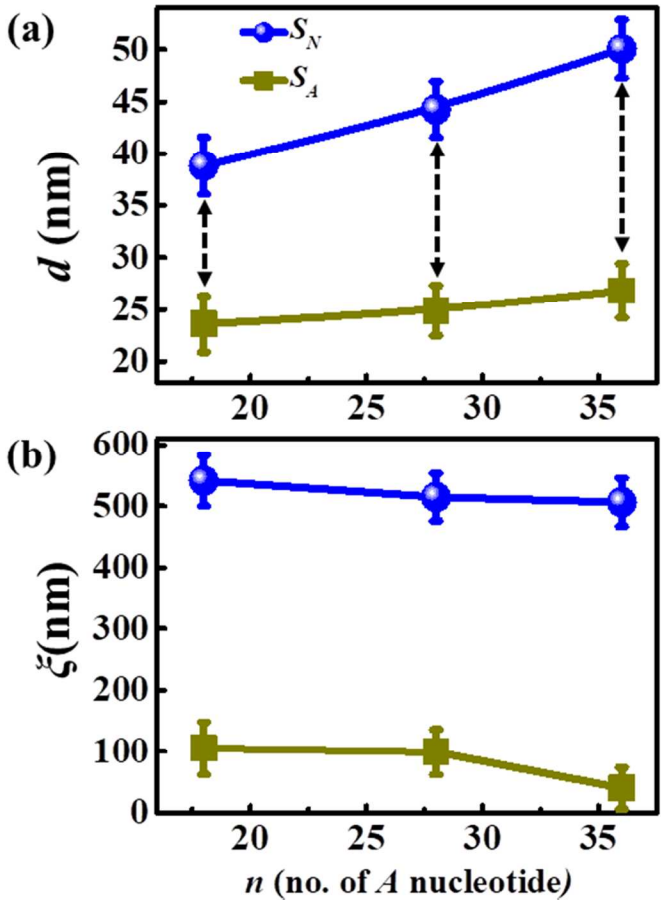


**Figure 4** (a) Observed in-plane nanoparticle distance, *d vs n*, the number of *A* nucleotides in the pH-responsive linker for the $S_N$ (●) and $S_A$ (■) states. With increase in *n,* the difference in the spacing, *d,* between $S_N$ and $S_A$ increases (b) The estimated correlation length $\xi^{A1}$ for the $S_A$ state reveals a reduced lattice order compared to the $S_N$ state.

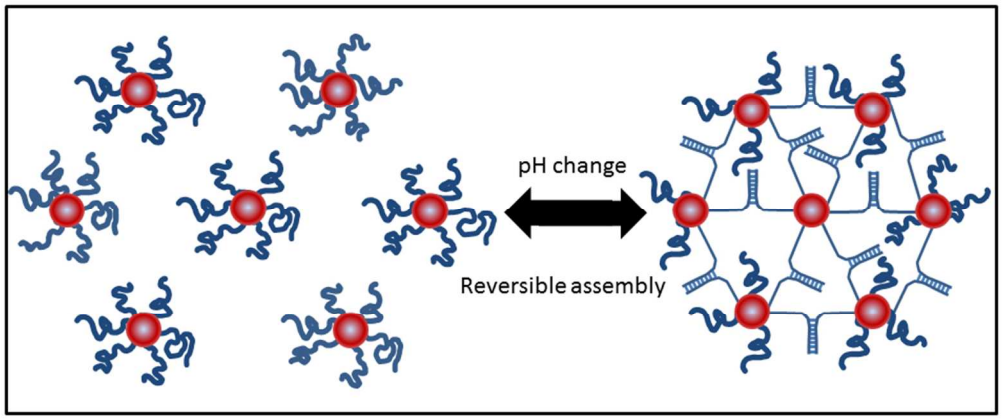


252x105mm (96 x 96 DPI)